Geant4 Simulations of Space Radiation Sensors and Environment At The Aerospace Corporation

M. D. Looper
Physical Sciences Laboratory
Space Sciences Department

November 28-30, 2018

Approved for public release. OTR 2019-00149.

© 2018 The Aerospace Corporation

Modeling sensors, shielding, secondaries…

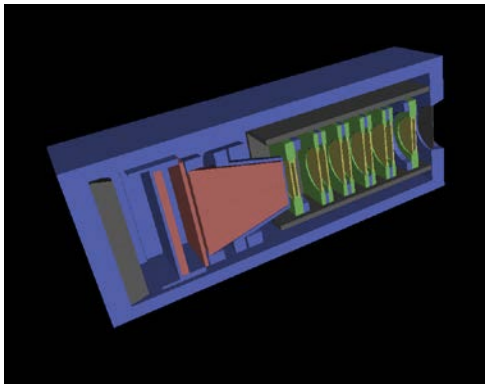

RPS (Relativistic Proton Spectrometer) aboard Van Allen Probes

Microdosimeters aboard AeroCube-6 (1/2U CubeSat)

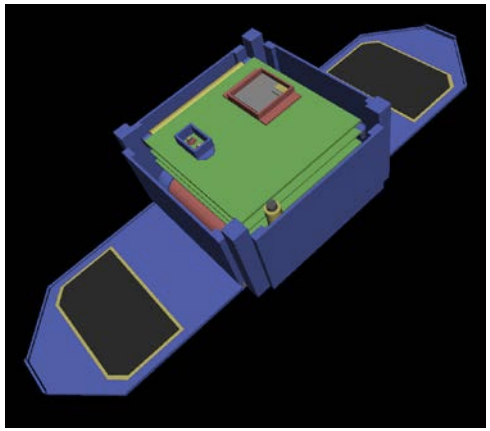

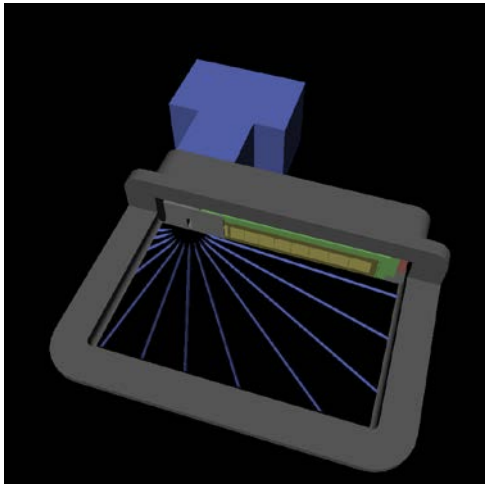

MagEIS (Magnetic Electron Ion Spectrometer) aboard Van Allen Probes

CRaTER (Cosmic Ray Telescope for the Effects of Radiation) aboard Lunar Reconnaissance Orbiter

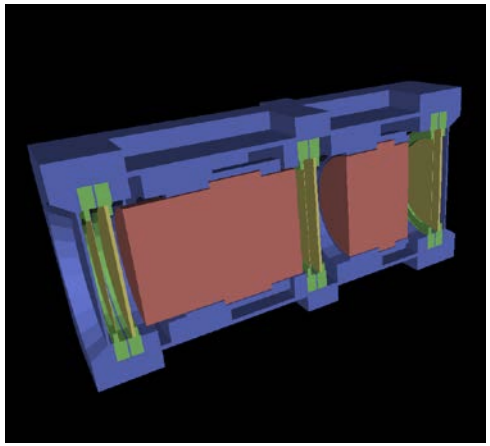

Since Last Year's Geant4 Space Users Workshop…

- We are continuing to work with foreground and background responses of sensors as on previous slide, and data from flight units, *e.g.*:
  - *MagEIS: Hartinger et al., GRL, doi: 10.1029/2018GL080291*
  - *MagEIS: Claudepierre et al., JGR, submitted, others in preparation*
  - *MagEIS: Looper, Aerospace Technical Report ATR-2018-1253*
  - *RPS: O'Brien et al., Space Weather, doi: 10.1029/2018SW001960*
  - *CRaTER: Schwadron et al., Planetary & Space Sci., doi: 10.1016/j.pss.2017.09.012*
- This year I wanted to focus on the details of two projects, one basic research and one applied, on which I've spent a lot of time lately:
  - *Lunar GCR albedo: Fall AGU meeting, paper in preparation*
  - *Efficient calculation of dose in small electronic part in the presence of a large shielding mass: Looper, ATR-2018-00052, -00953*
- ATRs are cleared for public release if you want a copy of any.

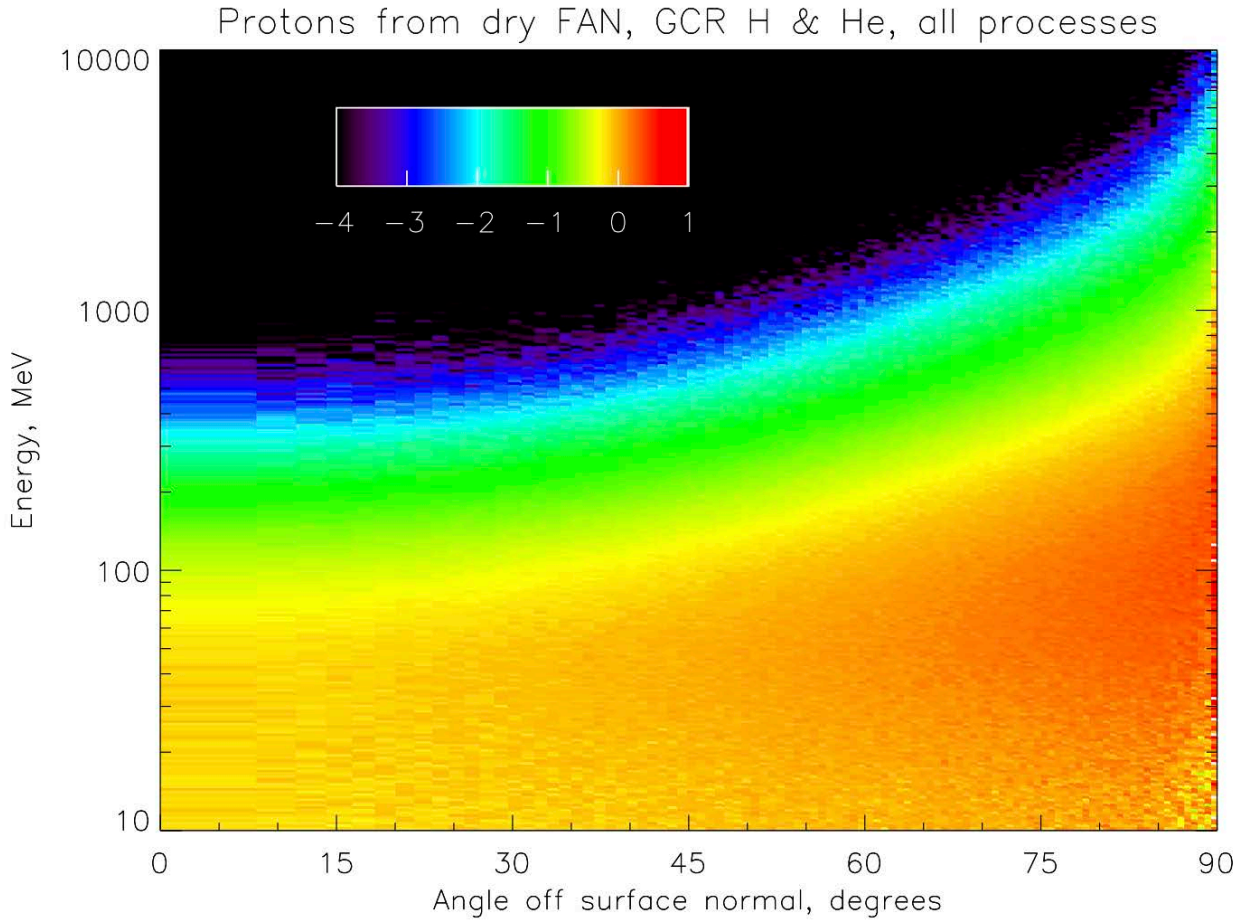

Using Geant4 version 10.04.p01, illuminate slab of ferroan anorthosite (FAN) with cosmic rays Z=1-28 (only H, He shown herein – others being processed) and tabulate “albedo” particles coming up from the surface. Focus on protons and neutrons observed by LRO; energy/angle distribution here for protons is typical for most species, with intensification and spectral hardening toward the limb (90 degrees). Colorscale is log flux in $(m^2\ sr\ sec\ MeV)^{-1}$. Look for differences from a surface with H or H_2O in upper layers above dry FAN.

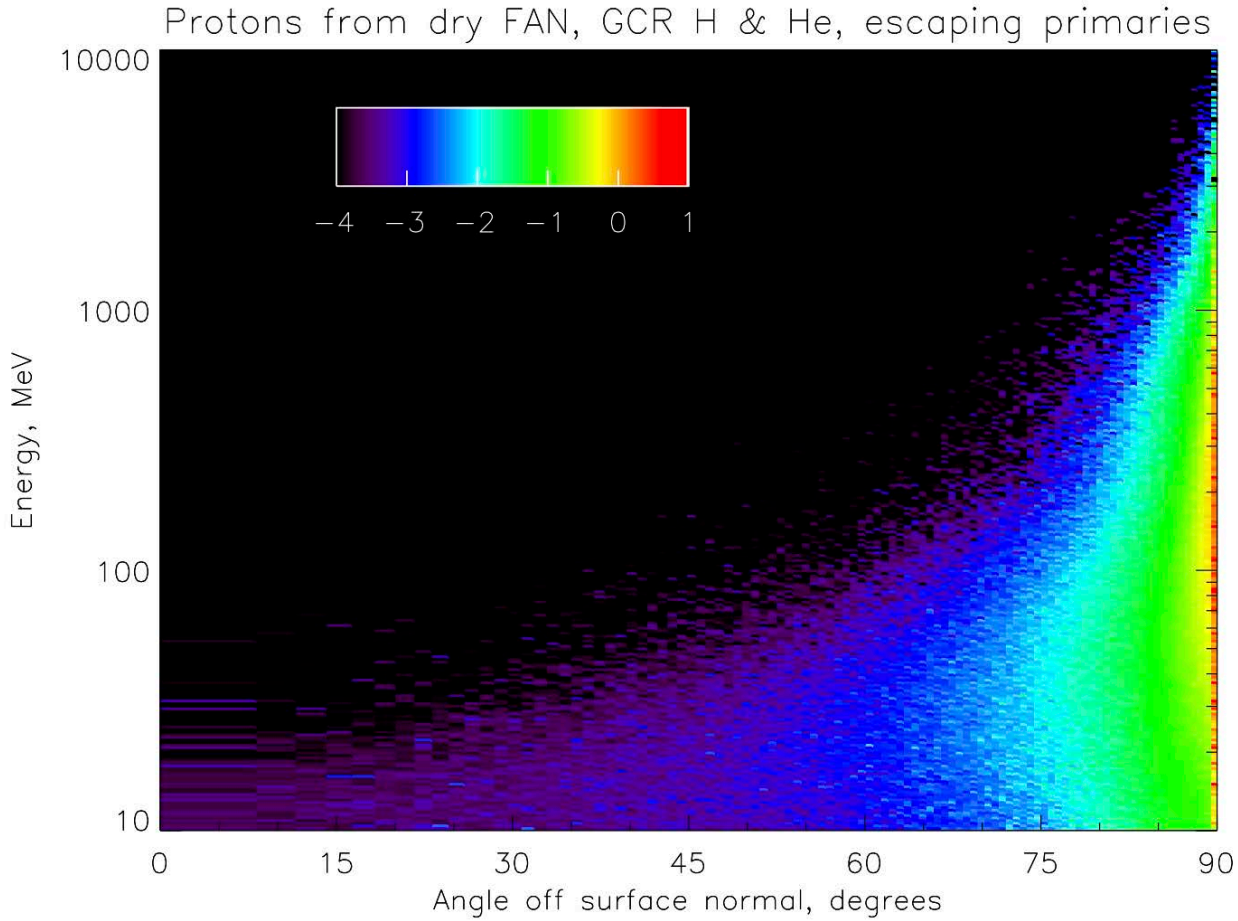

Geant4 lets us associate a source location and creation process with individual particle tracks. I divided these into elastic and inelastic ejection of secondaries, or escape of primaries after scattering. No discernible elastic contribution to protons or neutrons from dry FAN; most of previous plot was inelastically produced secondaries. However, there is a modest population of primary protons scrubbing off some energy and being deflected back outward, as here.

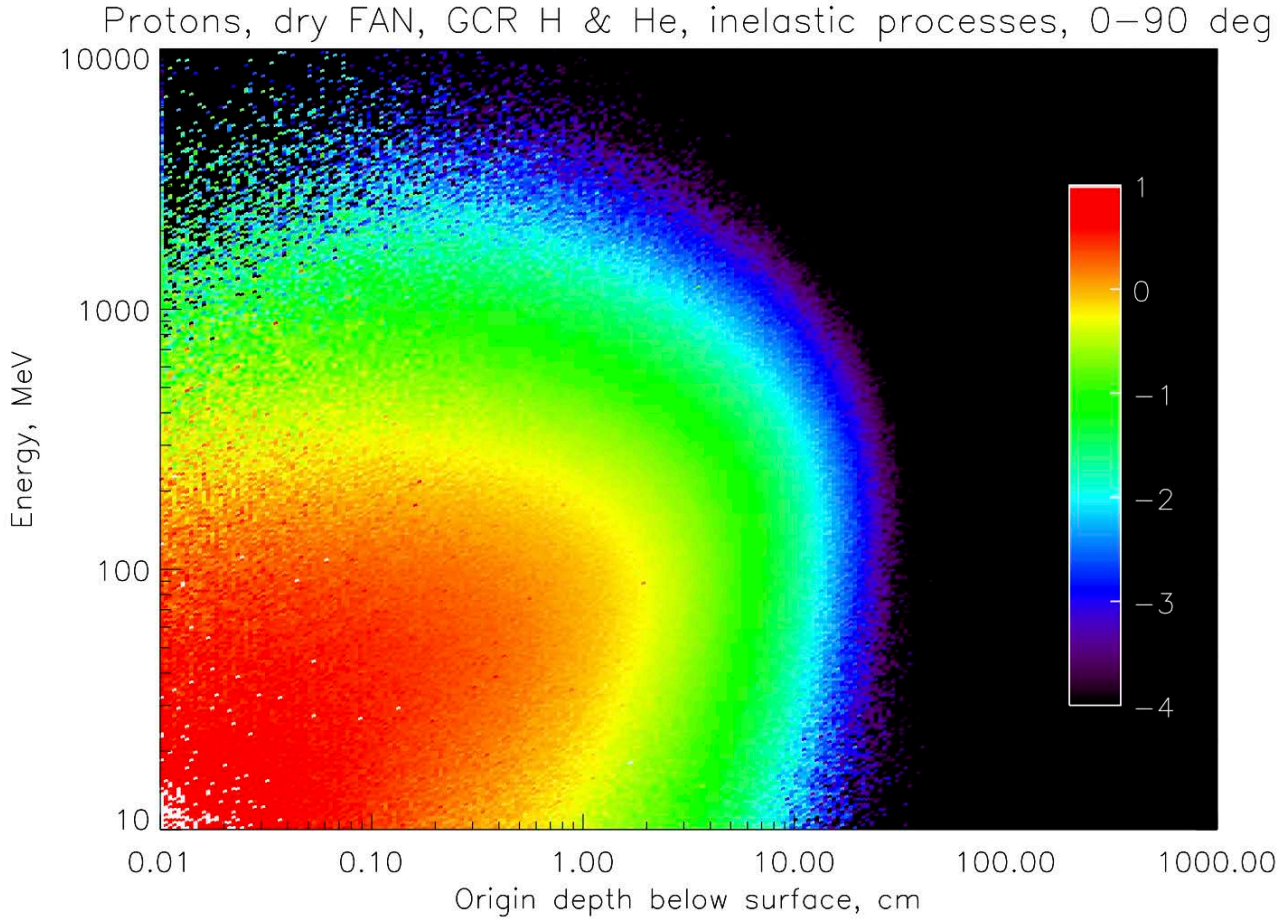

Here we plot the depth of origin of inelastically produced protons that escape the surface; colorscale is log of flux per cm of depth. Note correlation of depth with energy: more energetic protons tend to have probed greater depths. This plot integrates over all angles; plotting separate subsets of particles near vertical and near limb shows the expected pattern that the latter come from shallower depths due to greater oblique pathlength to escape. Discernible fluxes at these energies probe down to about 10 cm depth.

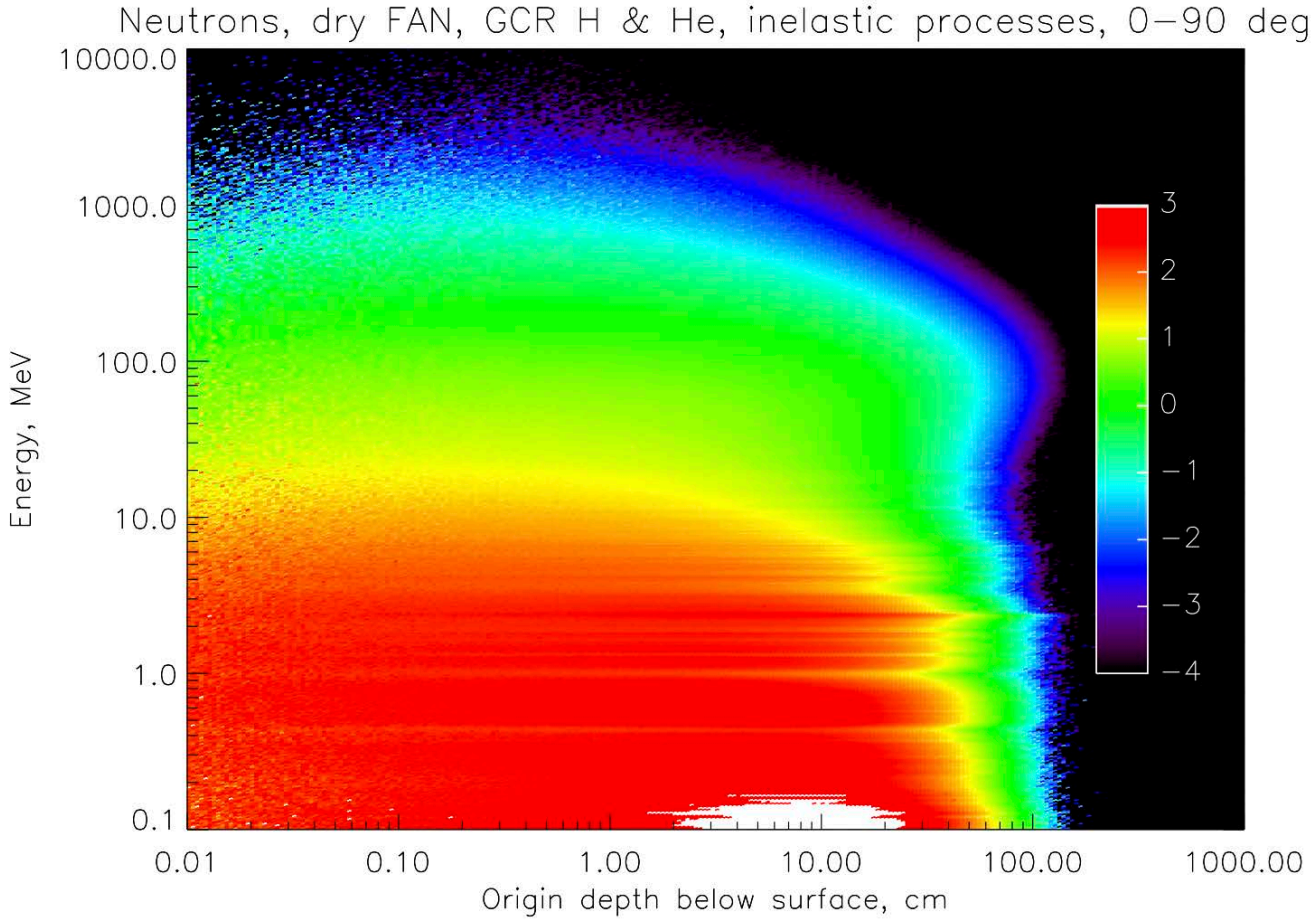

By contrast, neutrons are produced about equally from interactions at any depth down to the limits of penetration of the source GCRs, about a meter.

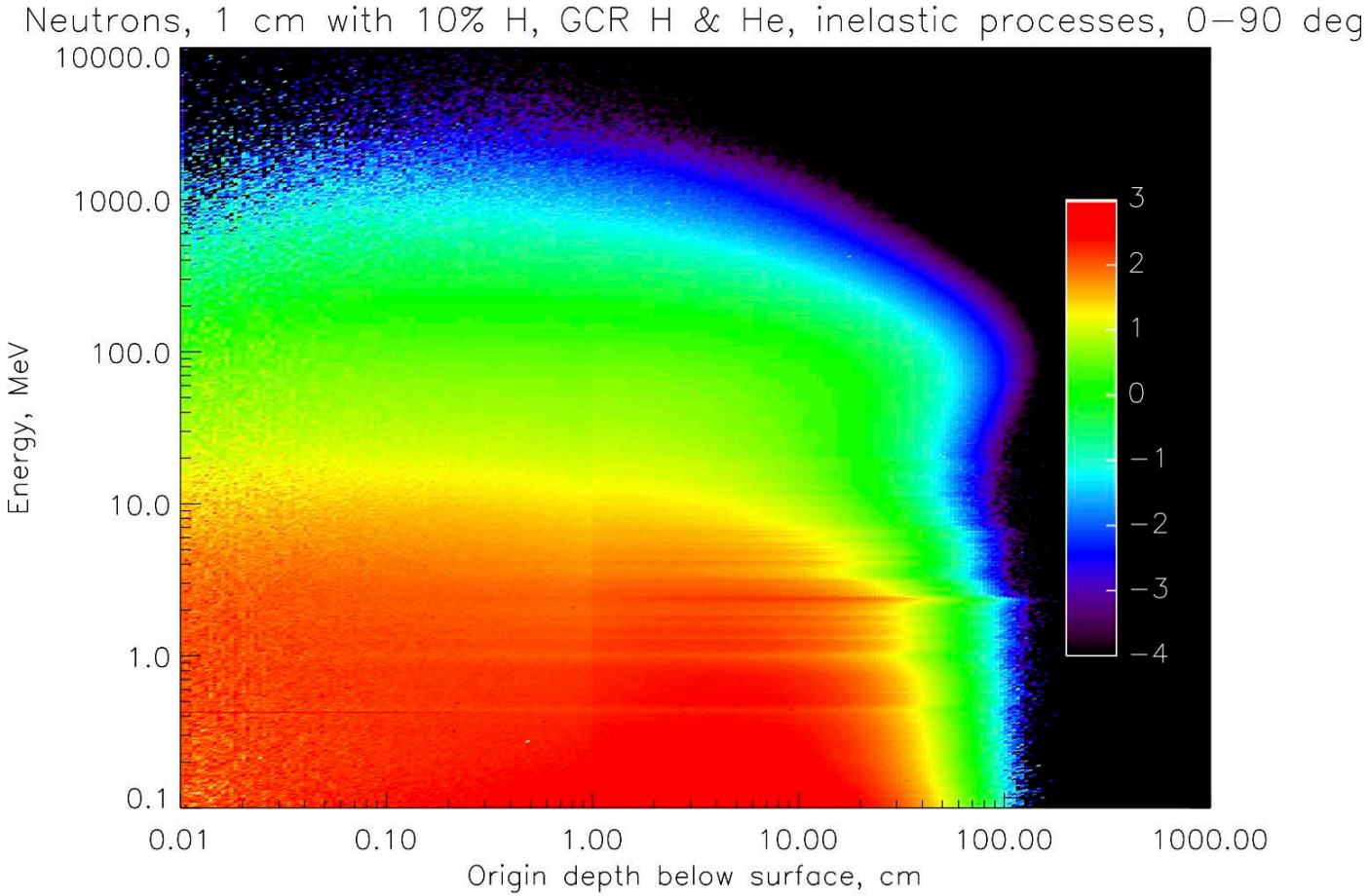

Adding a layer containing hydrogen filters the escaping neutrons, converting some of their energy to “tertiary” protons. Flux of neutrons generated below the hydrogenated surface layer is almost unchanged (not shown here in detail), but this plot only shows those that escape, which population is reduced. Note step at bottom of hydrogenated layer, as (slightly) lower average Z within that layer relative to below it reduces generation of secondary neutrons.

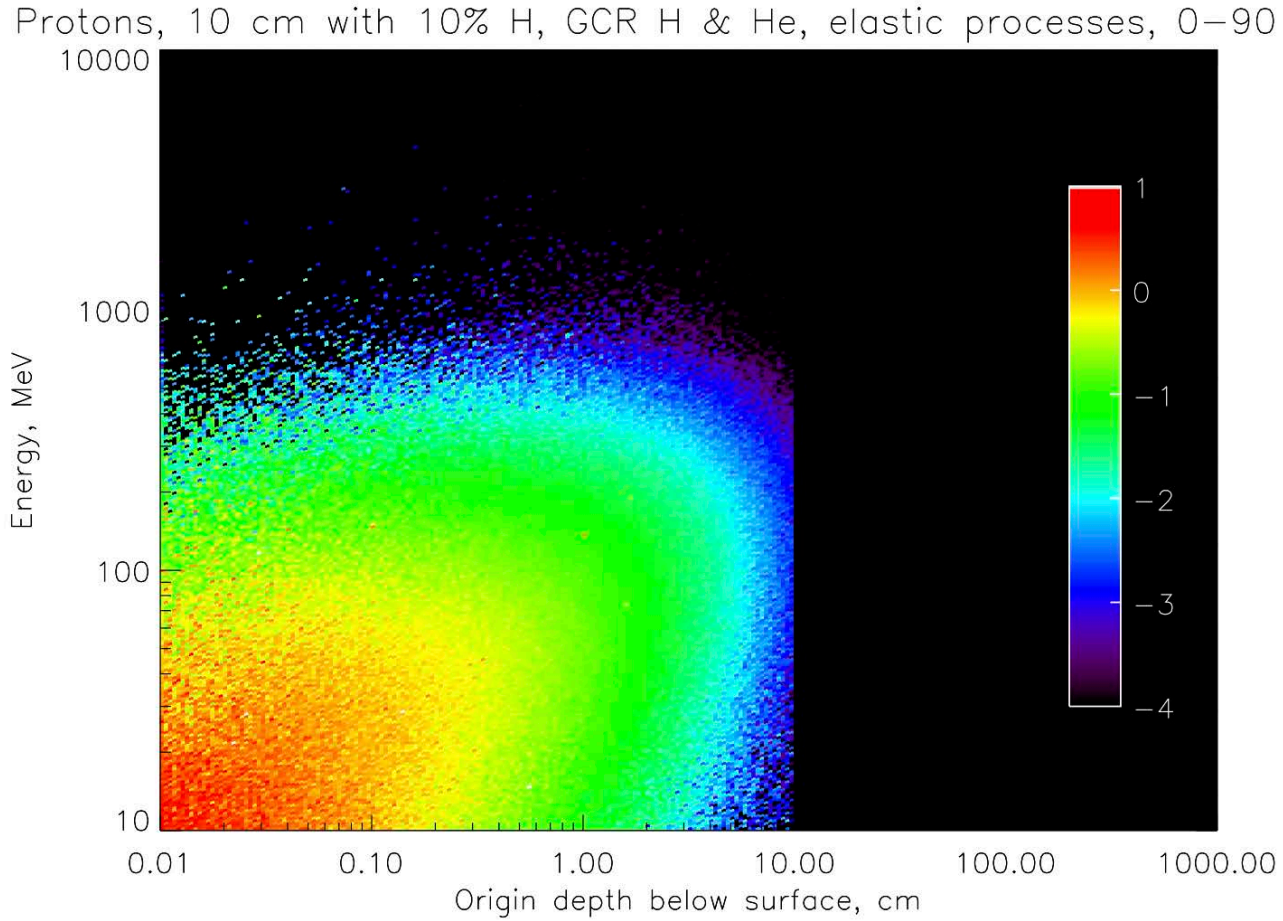

Elastic scattering of neutrons on target protons in the hydrogenated layer results in a population of ejected protons, with energy/depth pattern similar to the inelastically produced protons (shown earlier for dry FAN), but clearly cut off at the maximum depth where hydrogen is present.

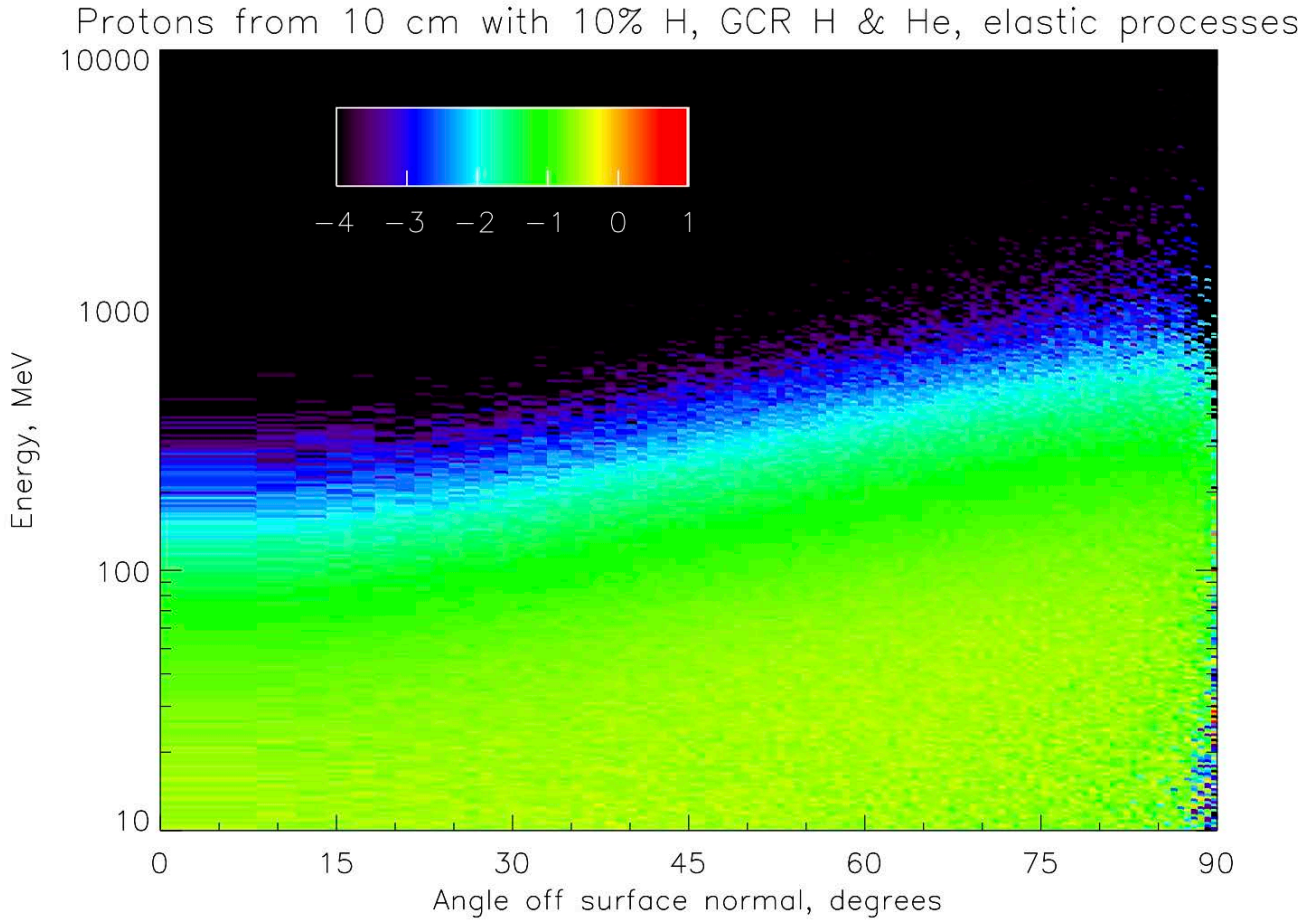

These elastically produced protons escape the surface at all angles and a range of energies, reflective of the broad energy/angle distribution of the upgoing neutrons that eject them.

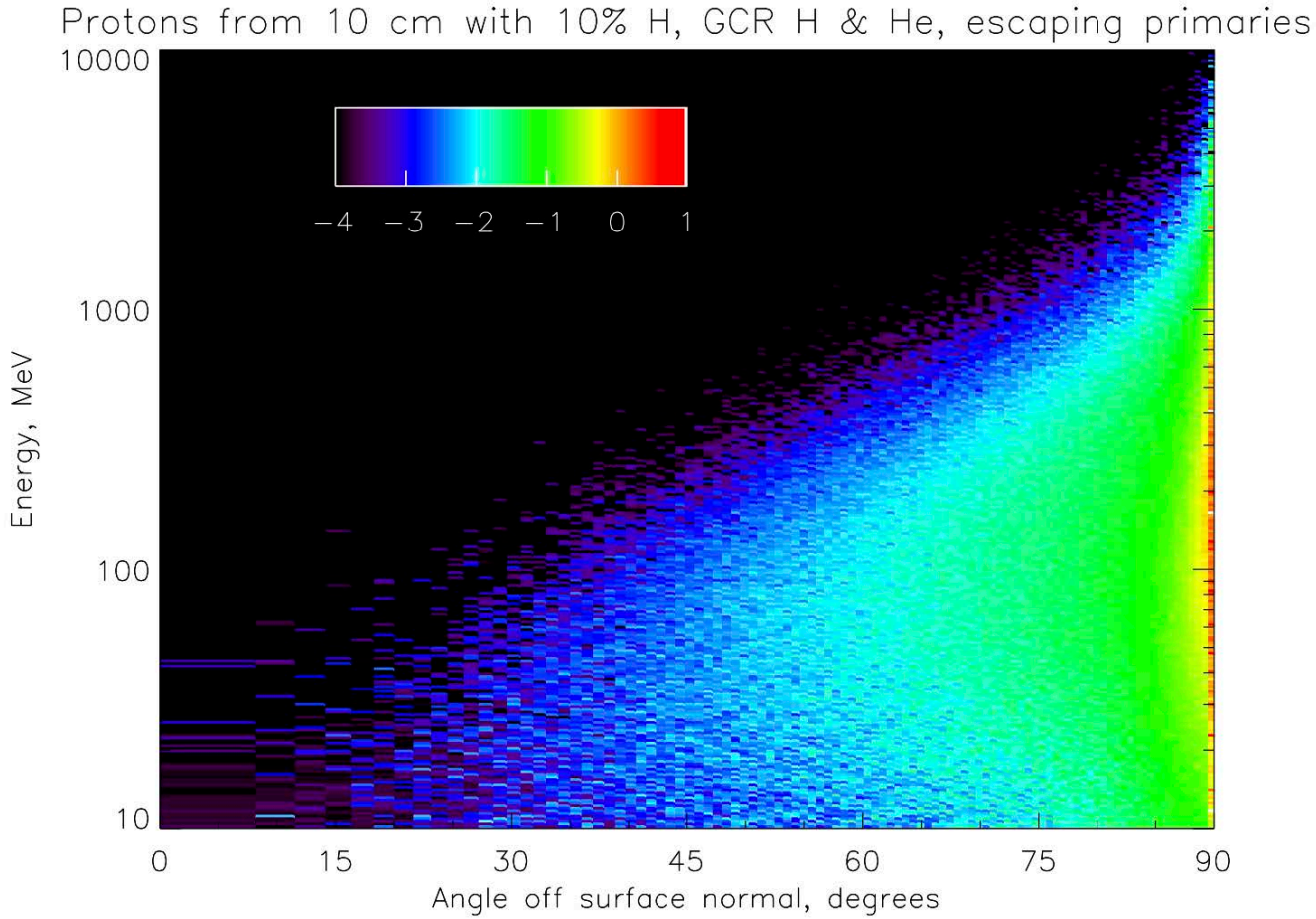

Addition of hydrogen in surface layers also enhances backscattering of primary protons, and sends them off at angles closer to vertical than from dry FAN.

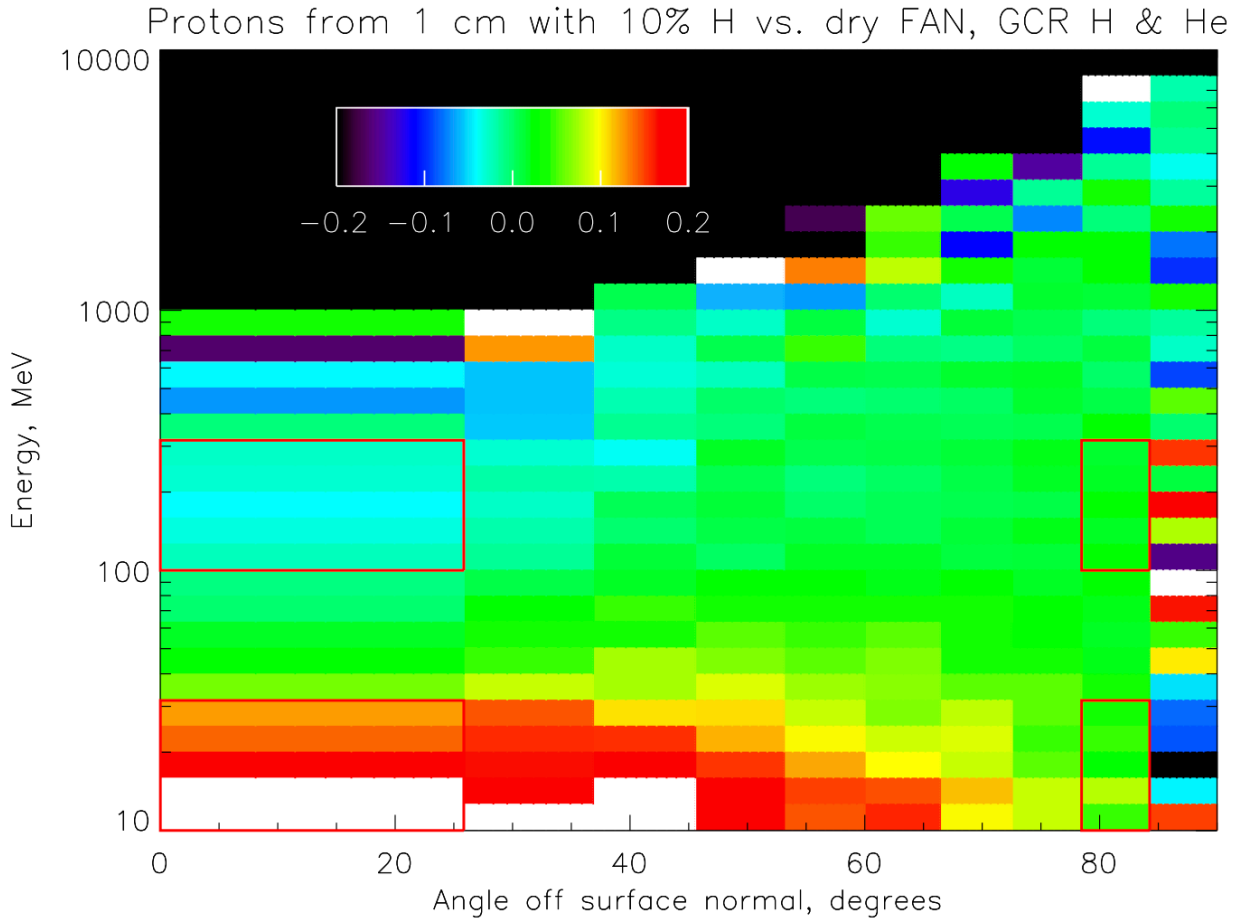

To show trends with hydrogenation fraction and depth, we form ratios between albedo coming from hydrogenated configurations vs. that from dry FAN. Colorscale is fractional difference relative to dry FAN. Energy and angle resolution is decimated here to boost statistics, but still very poor near the limb (90 degrees); four boxes enclose particles shown in subsequent plots, in two energy ranges and at angles seen looking toward nadir and toward the limb.

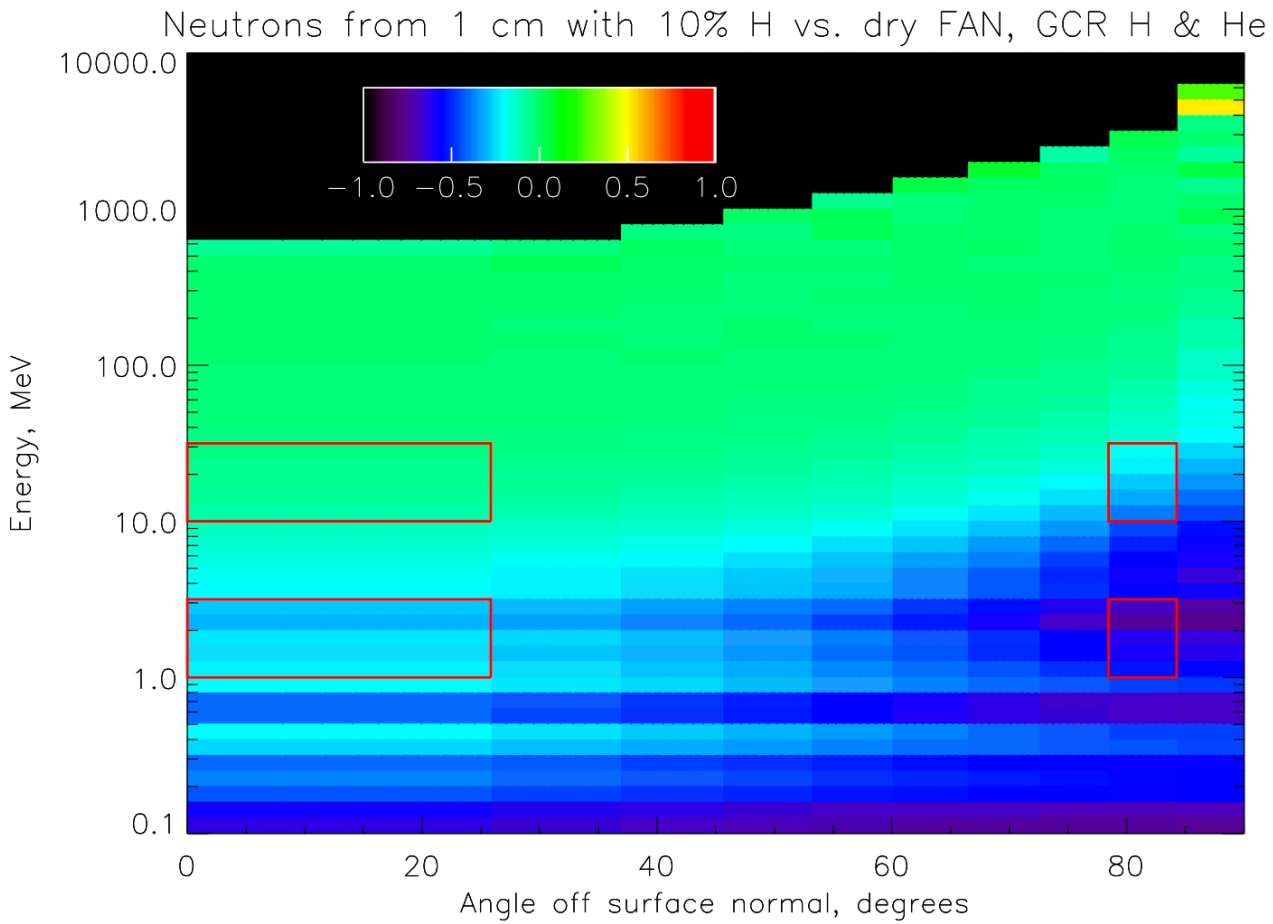

With no elastic ejection of secondary neutrons, their pattern is simpler, a reduction at all energies and angles, and though statistics are better than for protons we again sum up fluxes over the four energy/angle bins shown in red in subsequent plots.

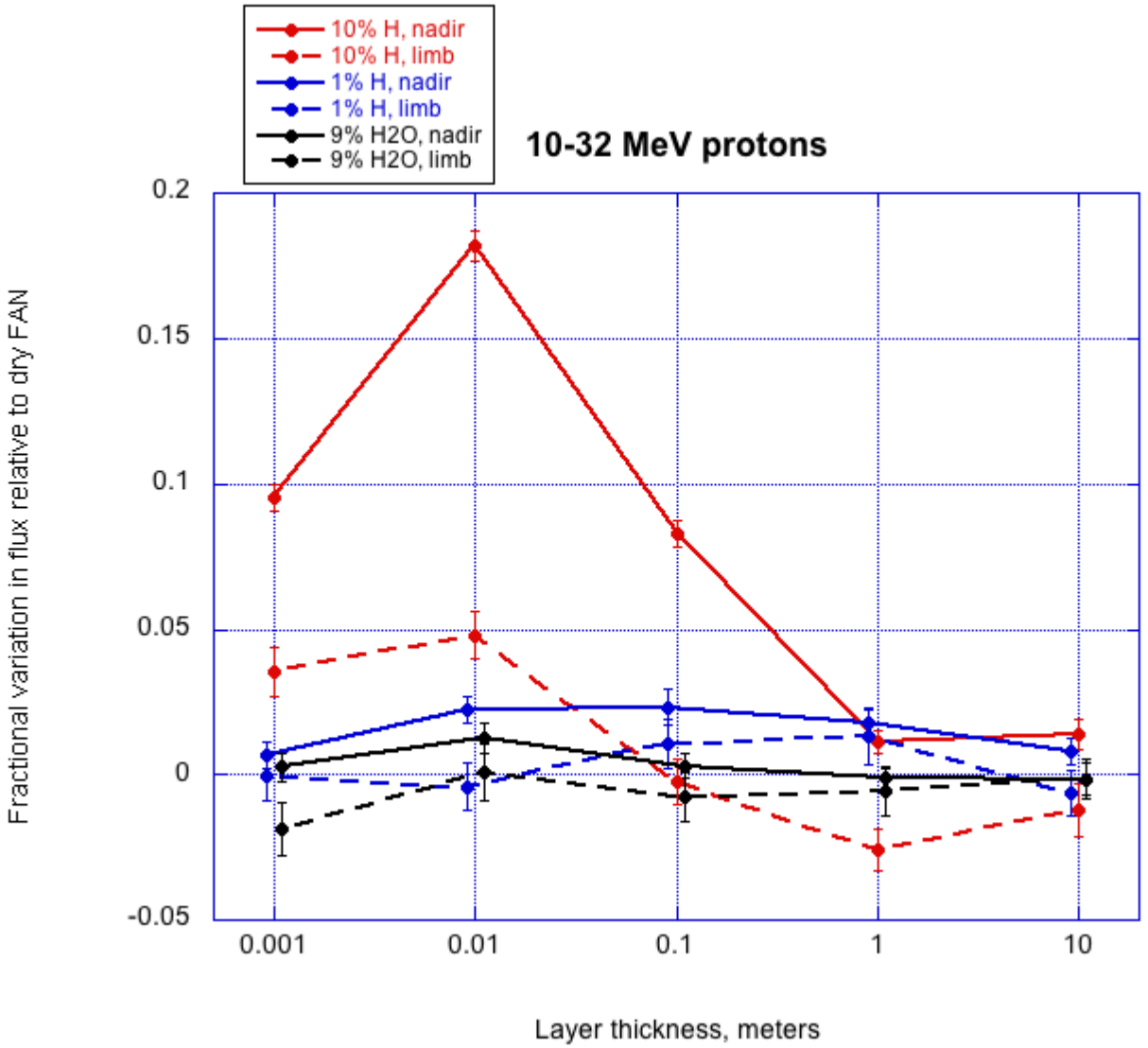

Five thicknesses of surface layer were simulated, with 10% or 1% H or 9% H_2O (1% H, 8% O) by weight. Here are the fractional enhancements of lower-energy protons; effects saturate by about 10 cm, and depletion of source neutrons for greater hydrogenated depths overcomes increase in hydrogen available for ejection. 1% H and 9% H_2O look similar, as expected.

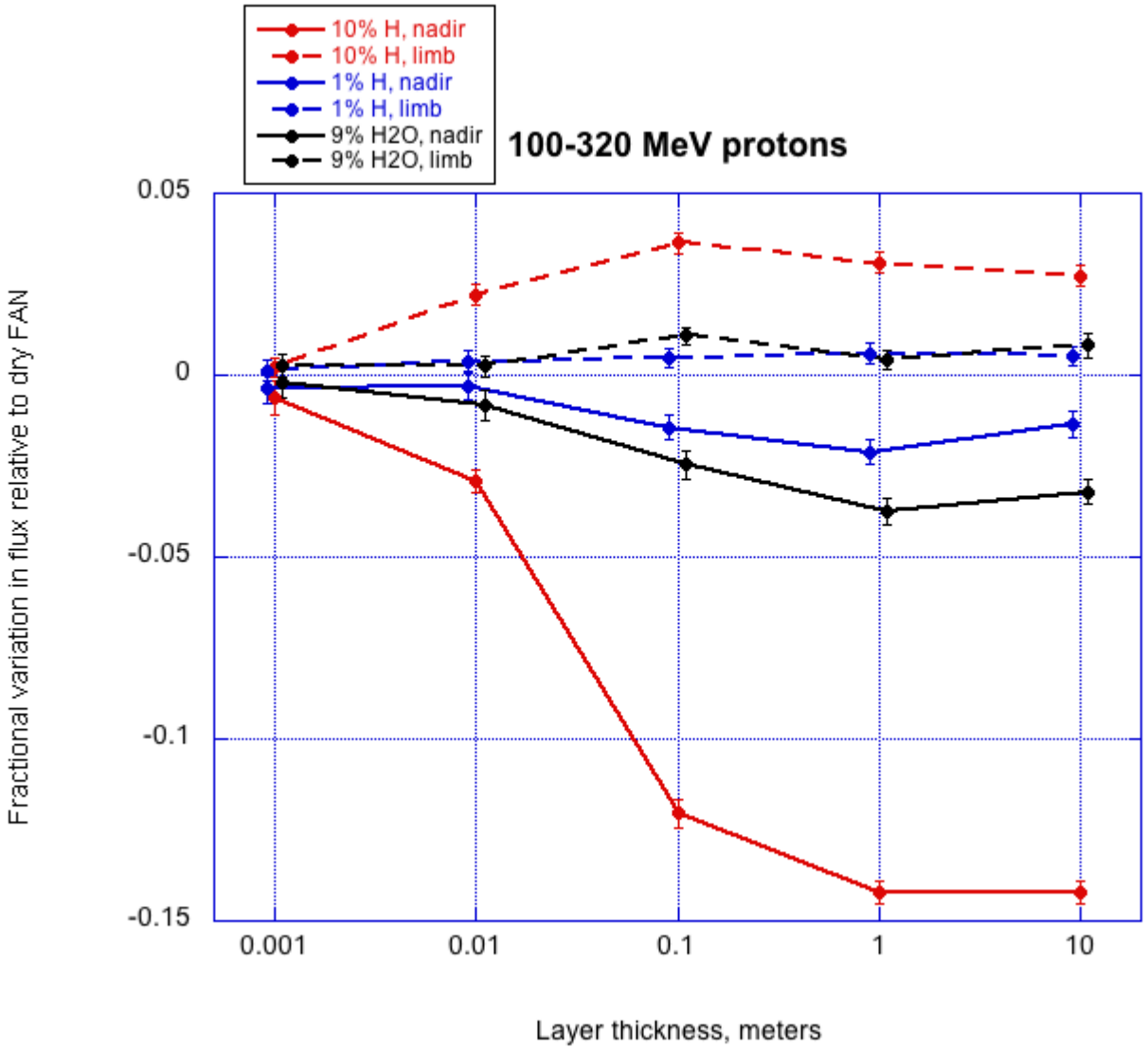

At higher energies, nadir-viewing (upgoing) protons are depleted throughout. CRaTER response for data channels analyzed in previous observational work is between these two energy bands; we are working to pin down the exact response to make a prediction like this for that specific channel, and are examining possibility of lower-energy observations.

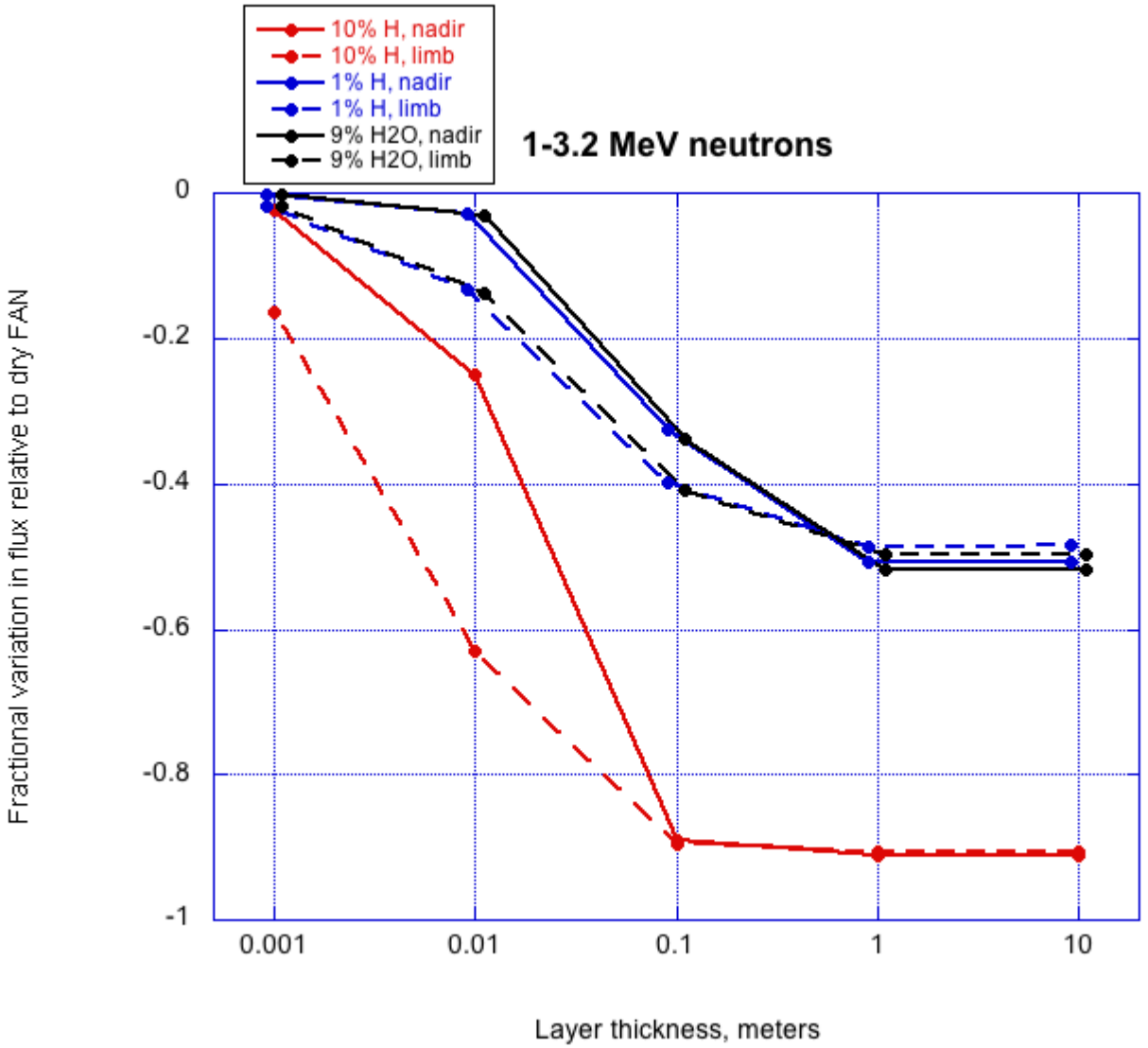

Neutrons show depletion throughout; higher-energy band looks similar but of lesser magnitude. Effects saturate by 1 meter depth; again, 1% H and 9% H_2O look similar, indicating that the further reduction in mean target Z due to the 8% oxygen in the latter doesn't much change things.

Dose In a Small Target Within a Whole Spacecraft

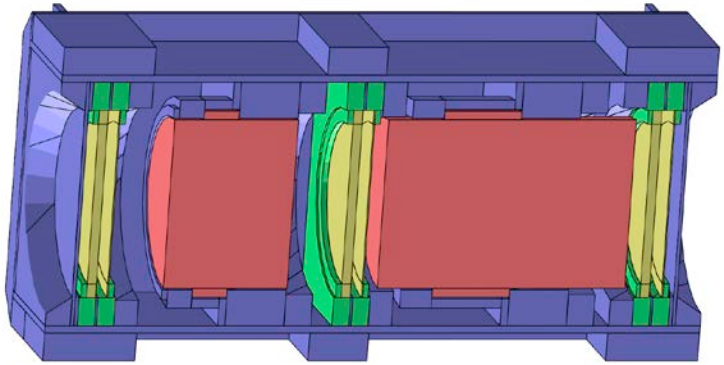

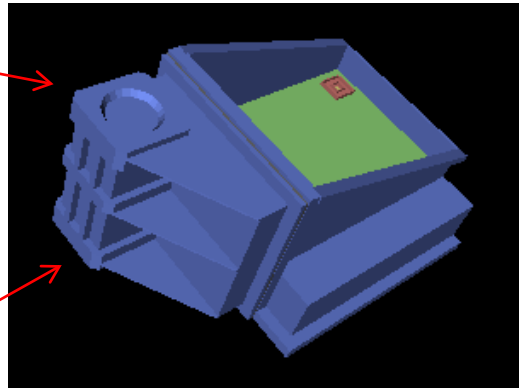

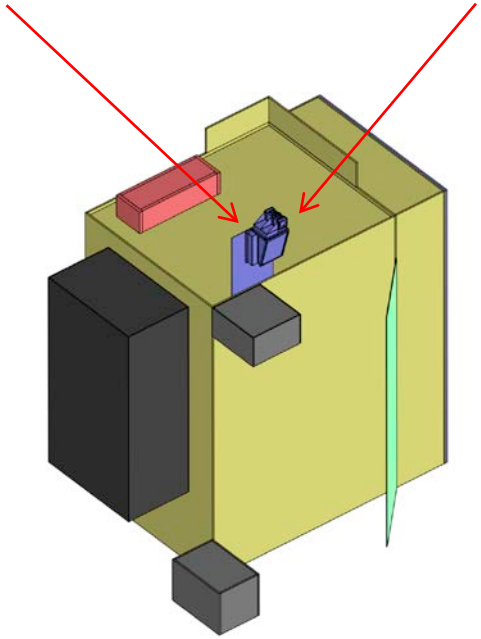

These nested Geant4 geometry dumps show the microdosimeter inside the electronics box (upper right) to scale against the whole LRO spacecraft.

It's inefficient to illuminate entire spacecraft with energetic particles in order to calculate dose in tiny chip inside microdosimeter using the standard forward Monte Carlo technique.

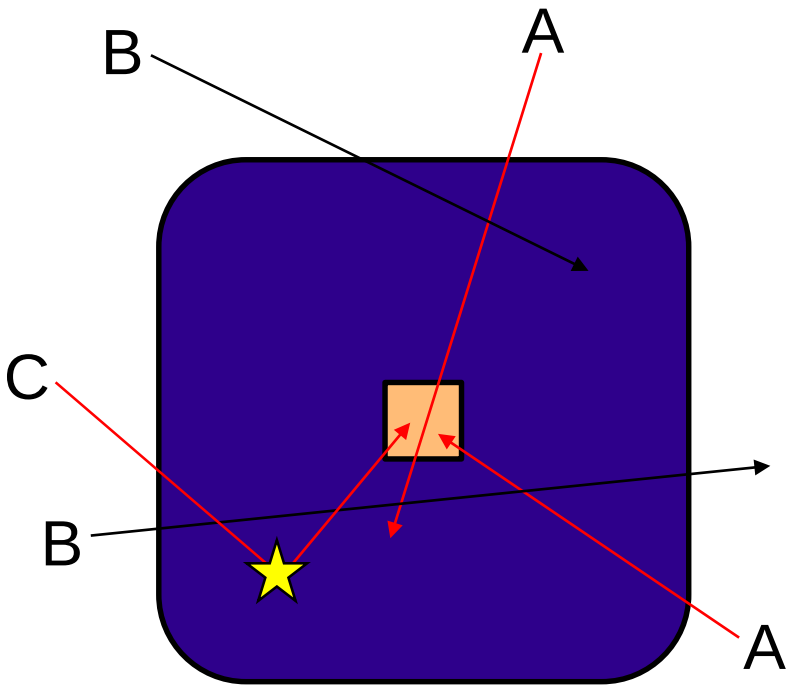

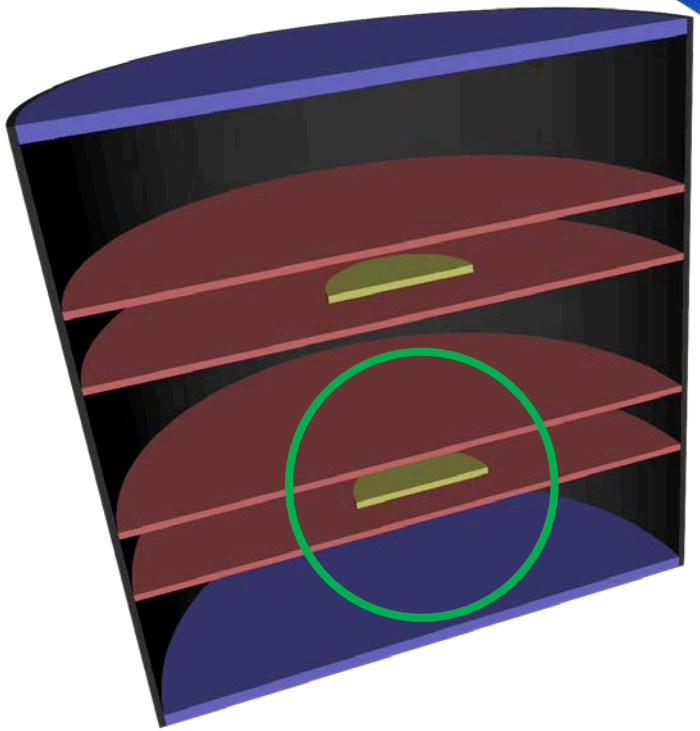

Forward MC simulates particles that travel through shielding to target like those labeled A, but in order to catch trajectories like C that scatter or send secondaries to the target despite not being aimed for it at the outset, it must waste lots of time simulating trajectories like B. Adjoint MC starts with (primary or secondary) particles at target, traces them probabilistically outward to source surface; catches A and C without wasting time on B. Sector shielding considers only A, tracing column mass density out along each ray from target and calculating that ray's contribution to dose from a dose-depth curve. Both techniques are much faster than forward; I evaluated them for one detector in the simple but representative geometry at right (yellow: silicon, red: Kovar, blue: aluminum, gray: Mallory) to compare results among techniques.

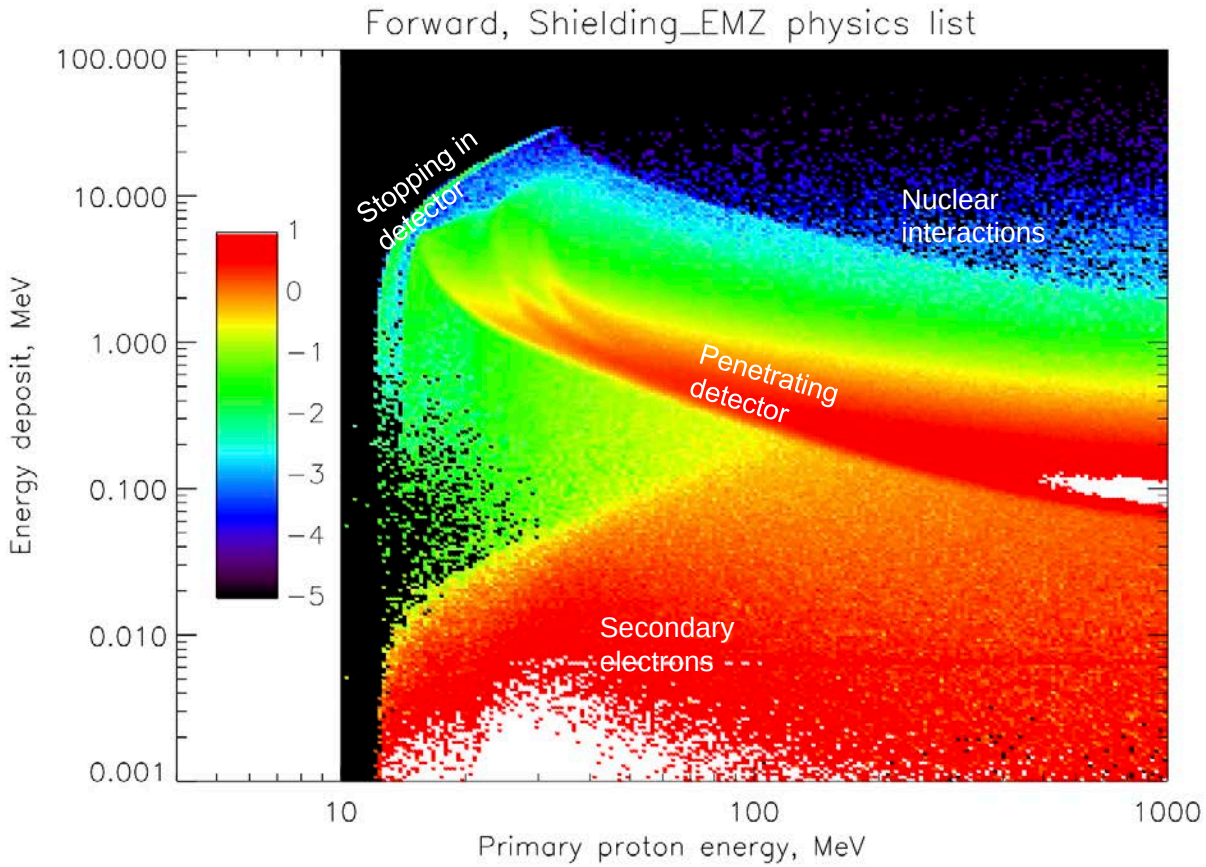

This and the next few plots show energy deposit response of one detector of this simple geometry for individual primary proton energies, with the colorscale showing log of response in (cm^2 sr) per MeV of deposited energy. Forward and adjoint simulations for electrons were in good agreement, so I will just discuss protons here. This plot is for the forward Monte Carlo with my “go-to” physics list, including nuclear interactions of high-energy protons. Different subsets of the response are as labeled.

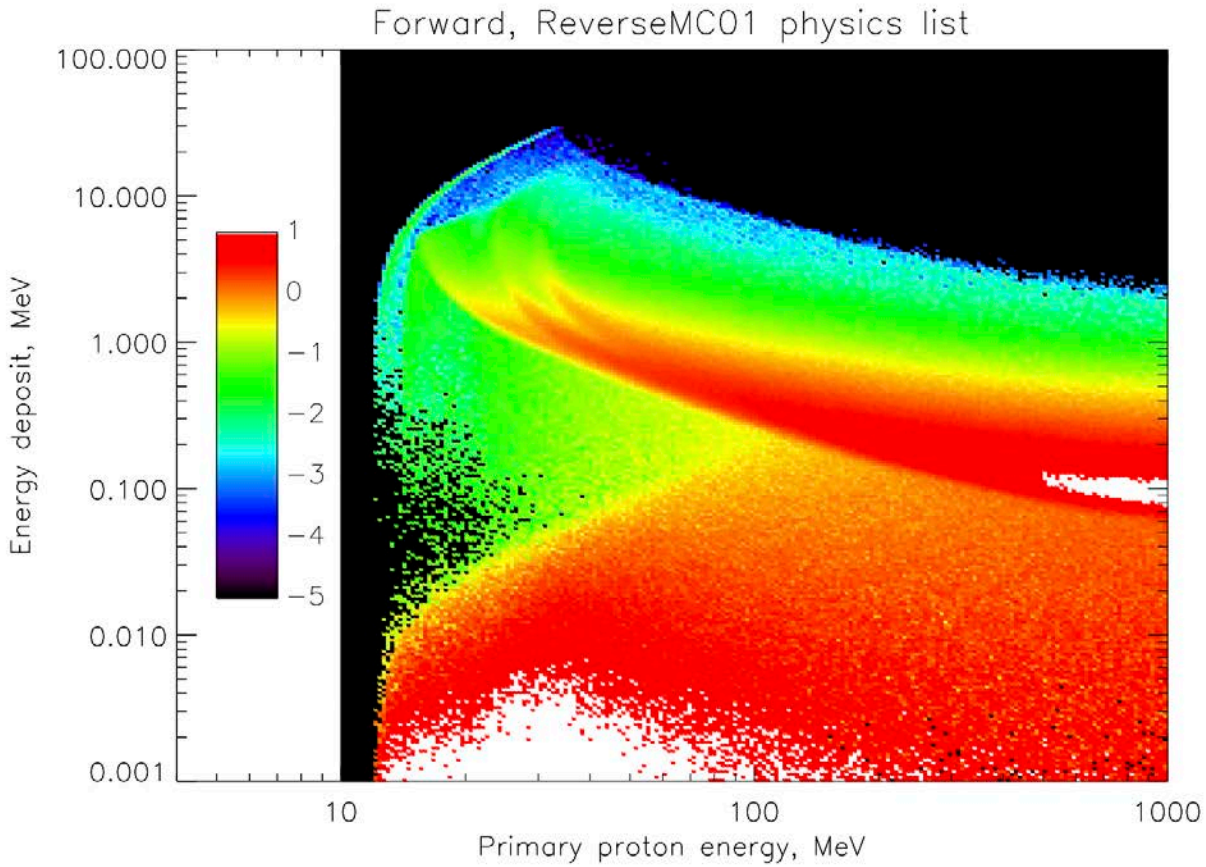

The adjoint Monte Carlo technique as implemented in Geant4 only considers electromagnetic interactions. The final step of this implementation does a small forward MC calculation within the designated target region (based on particles reaching its surface through adjoint transport), and this is the result of a full forward simulation using that EM-only physics list. Agreement looks good, except to upper left where high-energy protons start having nuclear interactions that this physics list does not model.

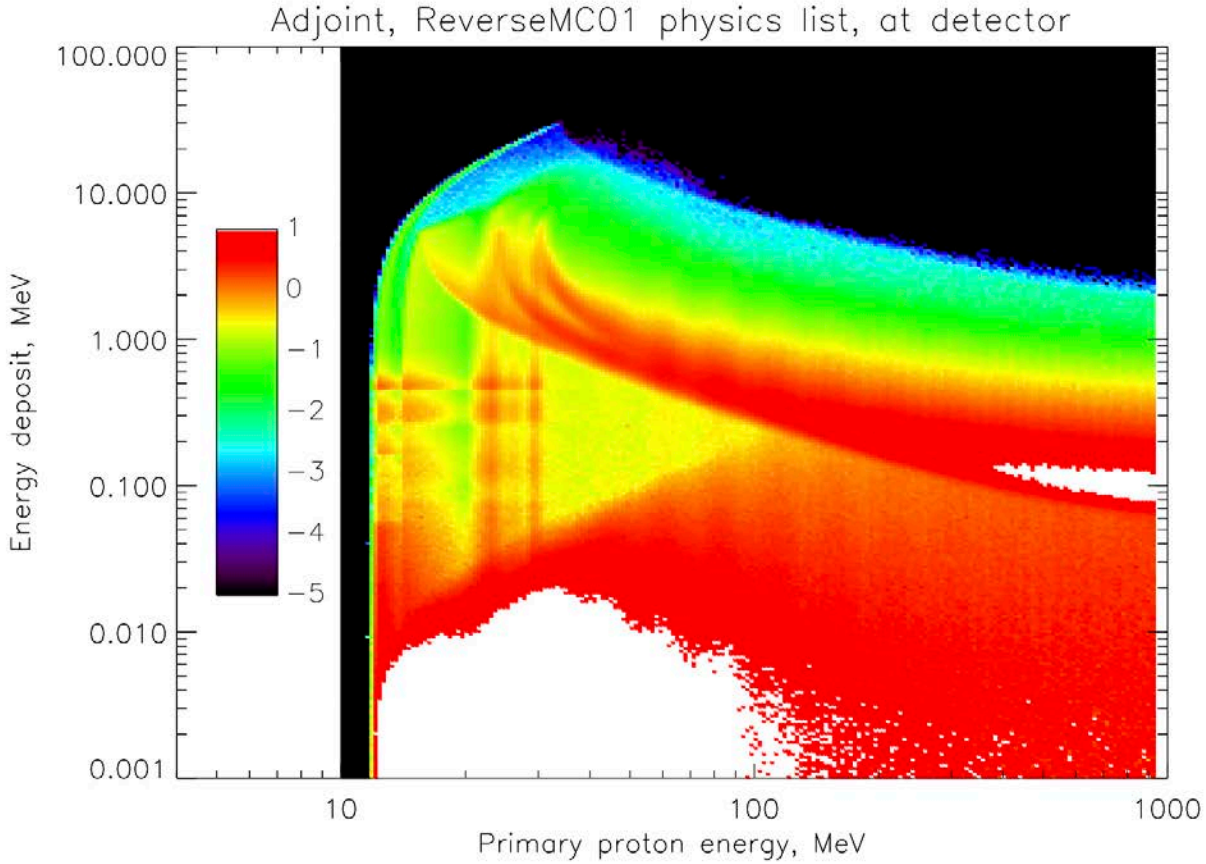

Considering the adjoint simulation, however, we find a much higher response than was calculated using the forward technique. There is also an odd wave pattern at intermediate energies (low-intensity vertical stripes) that I am at a loss to explain. A vertical cut through this plot would be the energy deposit spectrum for the given primary energy.

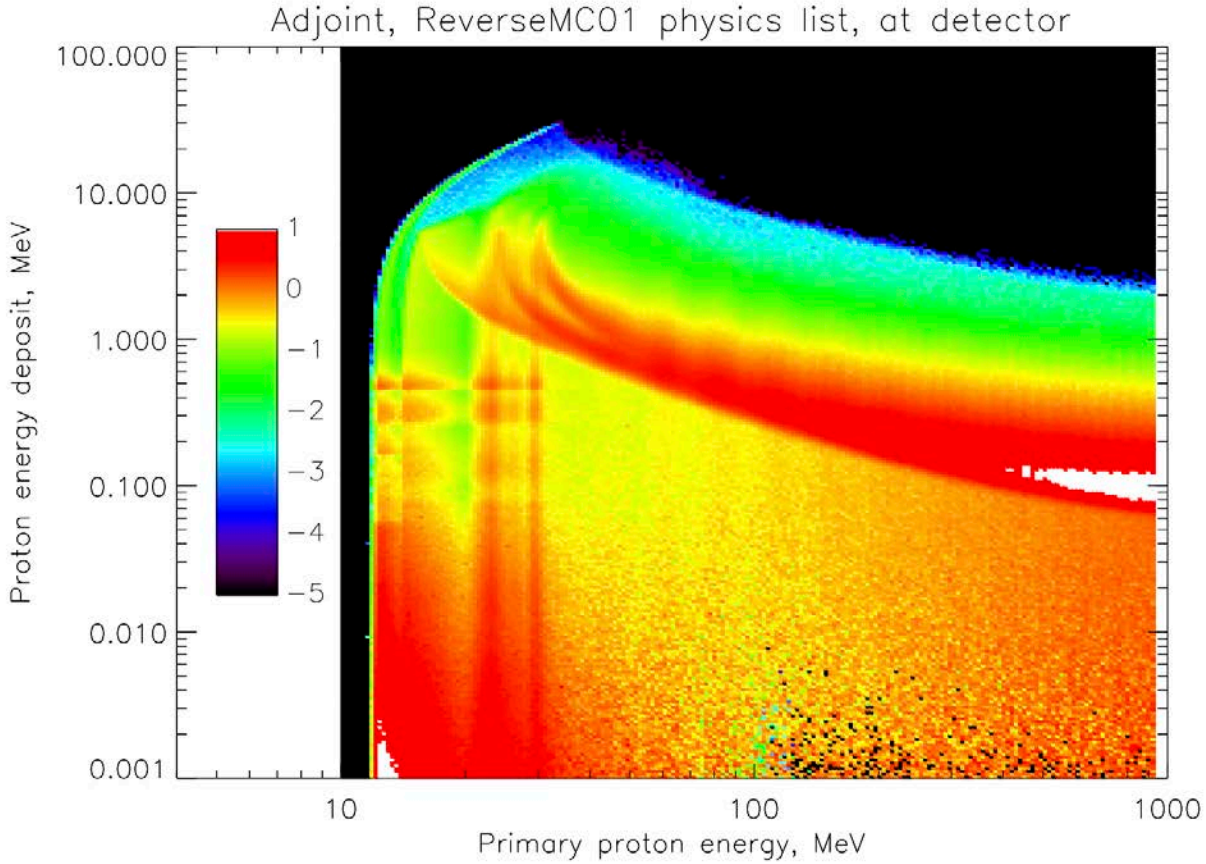

Since the adjoint technique starts particles at the target (here, the surface of the detector), we can focus only on energy deposits mediated by particles of a given species. These are simulated energy deposits due only to protons reaching the detector; the broad swath due to secondary electrons at lower left is omitted, uncovering a lot of extra response in vertical bands, with very strange structure along the bands.

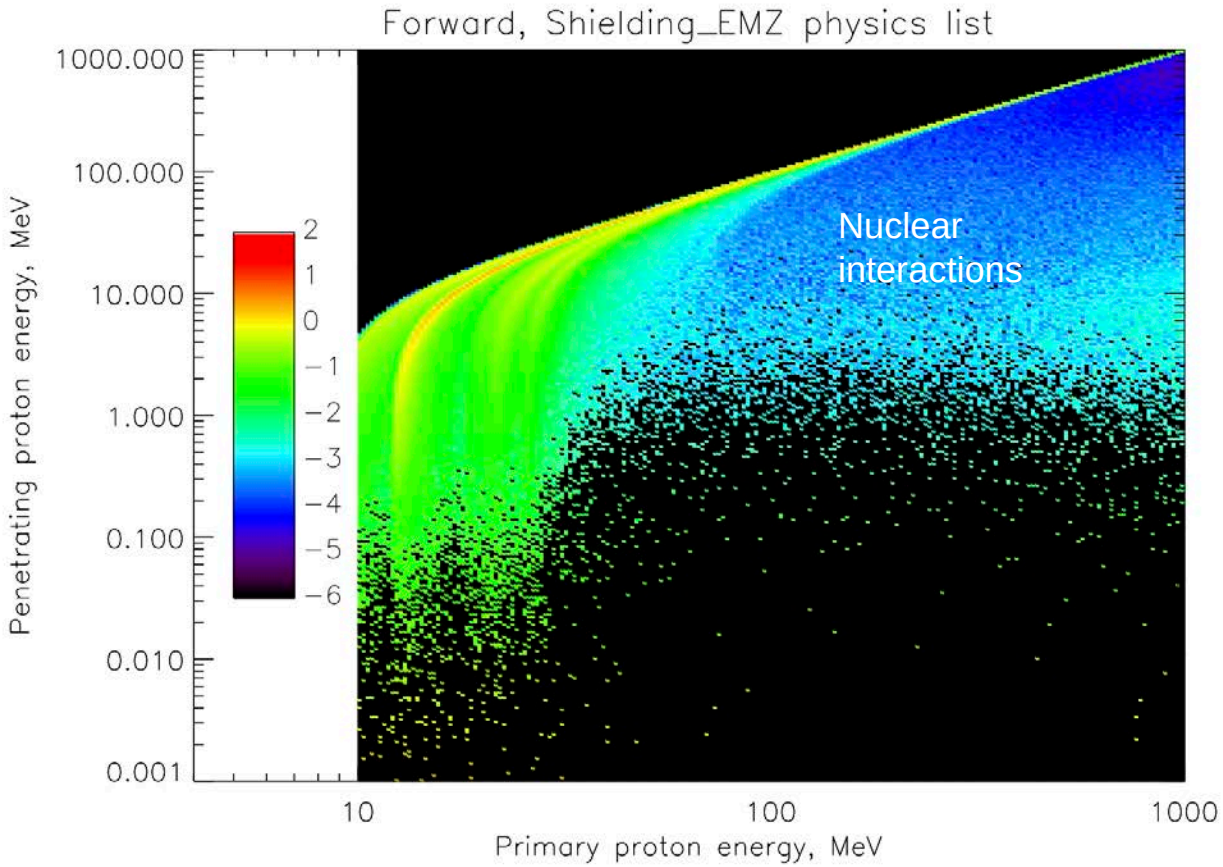

Another way to examine this is to tabulate protons reaching the target, as a function of primary proton energy. Here are the results for the forward MC with a physics list including nuclear interactions; protons that give some energy up to these are clearly visible as a population below the main diagonal. Colorscale is log response per unit penetrating proton energy, in (cm^2 sr) per MeV.

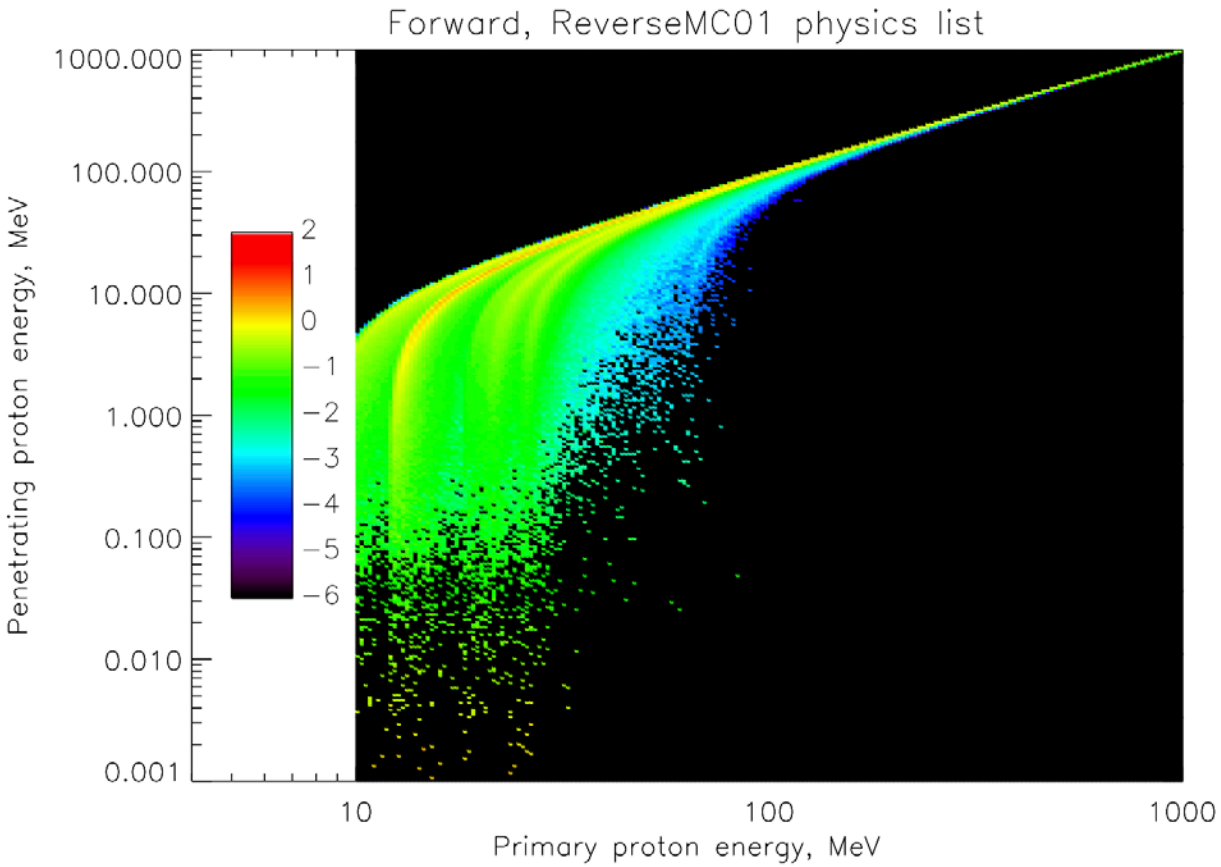

Using the EM-only physics list from the Geant4 example for the adjoint MC technique, we see very similar results except that the fan of reduced-energy protons below the diagonal due to nuclear interactions, as on the previous slide, is of course missing.

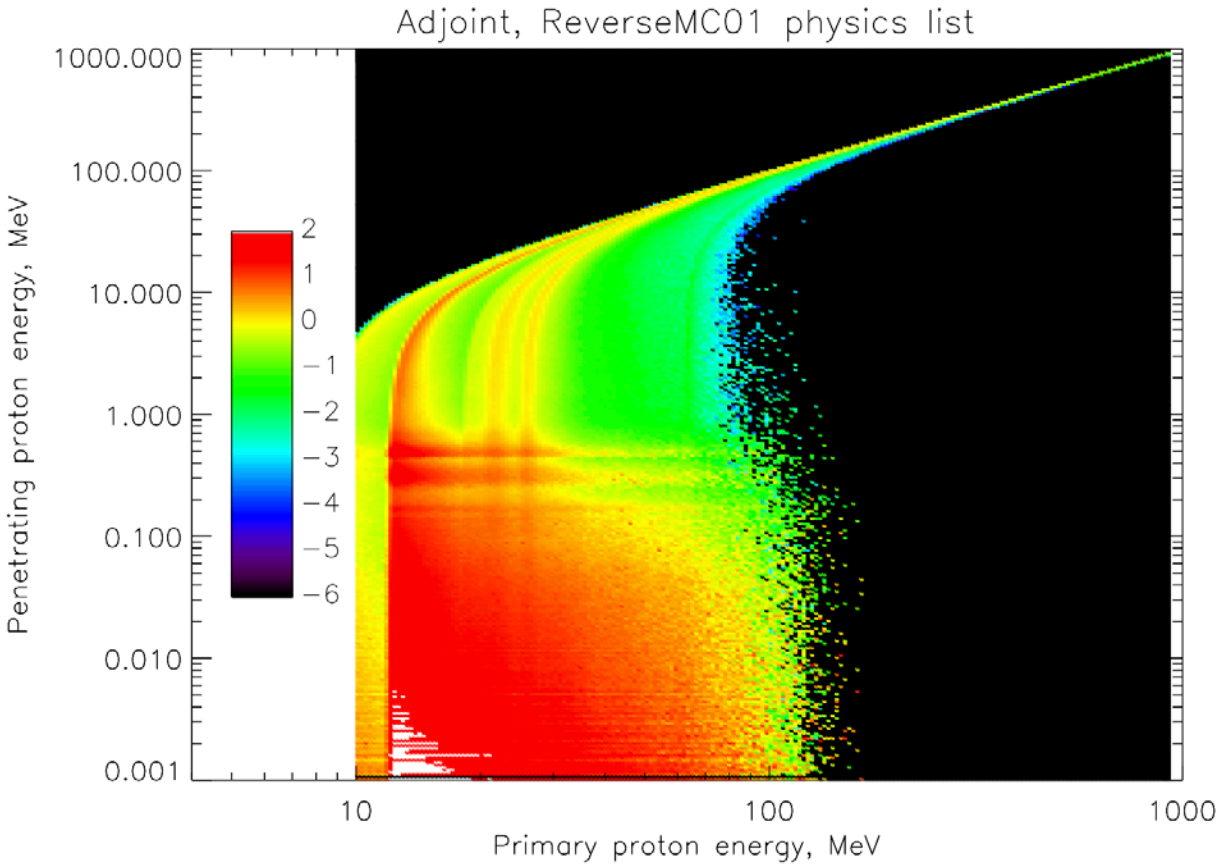

Going to the adjoint technique, we can see the origin of the peculiar structure in the energy-deposit plot a few slides back. There is a great increase in the number of low-energy protons (actually in the statistical weight assigned by the adjoint transport) at the detector surface. Thus, though we found the adjoint technique as implemented in Geant4 to be a good, faster substitute for a forward simulation of electrons, it is not an accurate substitute in the case of protons.

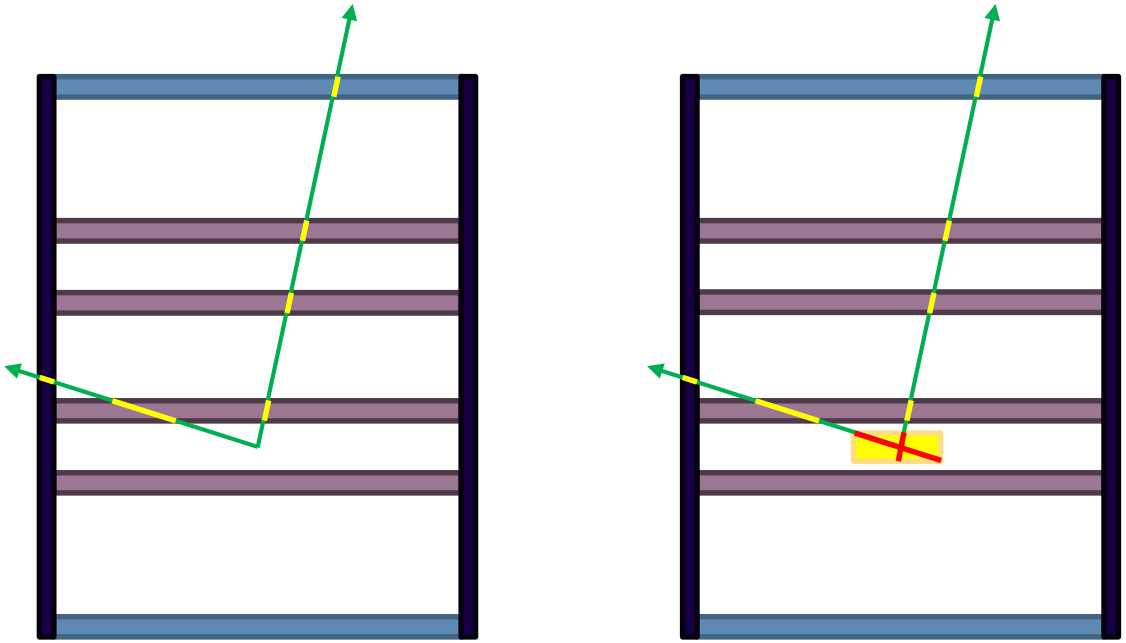

As an alternative for protons, we investigated the sector shielding technique. Typically a column density, or equivalent thickness of a fiducial material (usually aluminum), is calculated along each ray outward from a point, as at left, and then the contribution to dose from that part of the field of view is looked up in a dose-depth curve in the fiducial material. This does not account for variation of pathlength in the detector, so we modified the technique by tracing each ray back through the solid detector as at right, and using the CSDA (continuous slowing-down approximation) of protons, or equivalently a deterministic range-energy tabulation, to calculate individual energy deposits. The sum will give the same answer as the standard calculation, but individual “pulse heights” can also be calculated using this modified technique, which can be useful if, say, a microdosimeter has a threshold below which it does not count energy deposits.

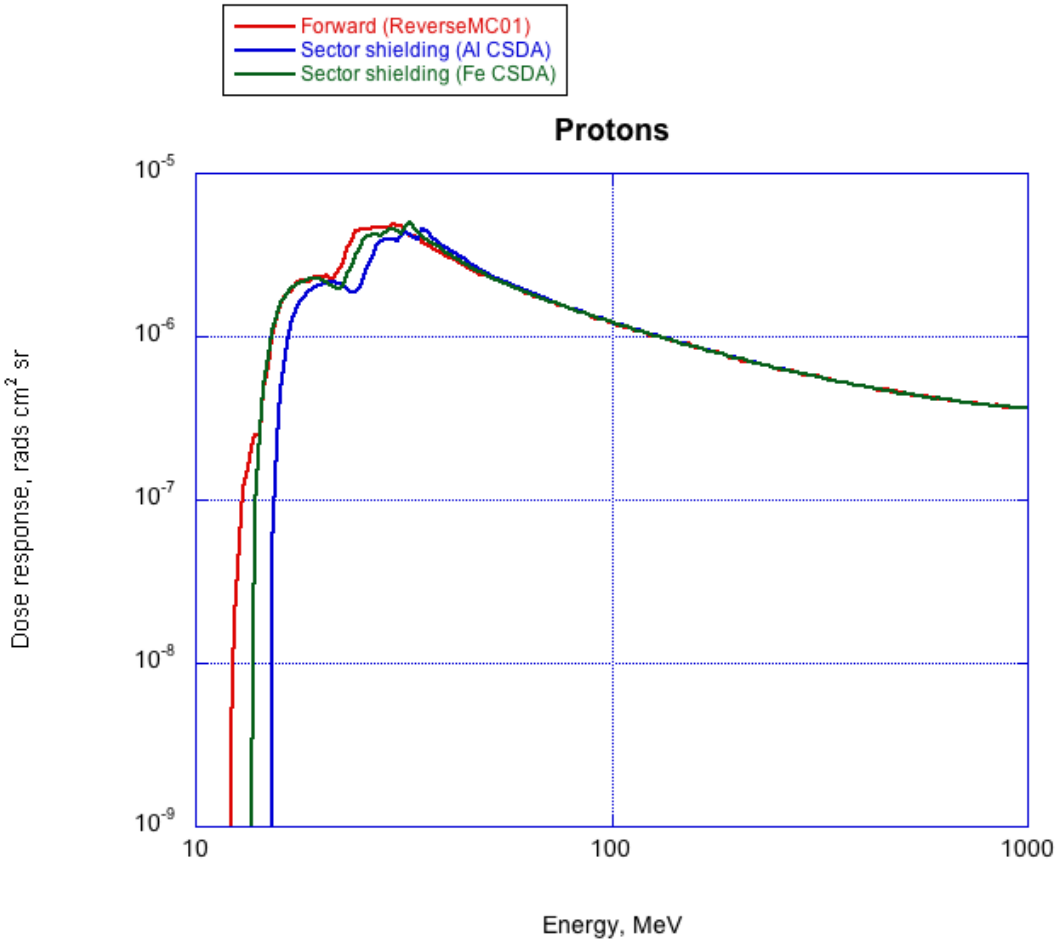

These curves represent an integral along each vertical stripe in the previous energy-deposit response plots, to make for easier comparison. We found that, while the sector shielding calculation gave a response with generally the same features and magnitude as the forward calculation (red curve, using the EM-only physics list), deviations are visible from the approximation that range-energy relation is the same for all materials when expressed as a column density. Using a different fiducial material, say iron, improves agreement where there is a lot of Kovar in the path, but worsens it elsewhere.

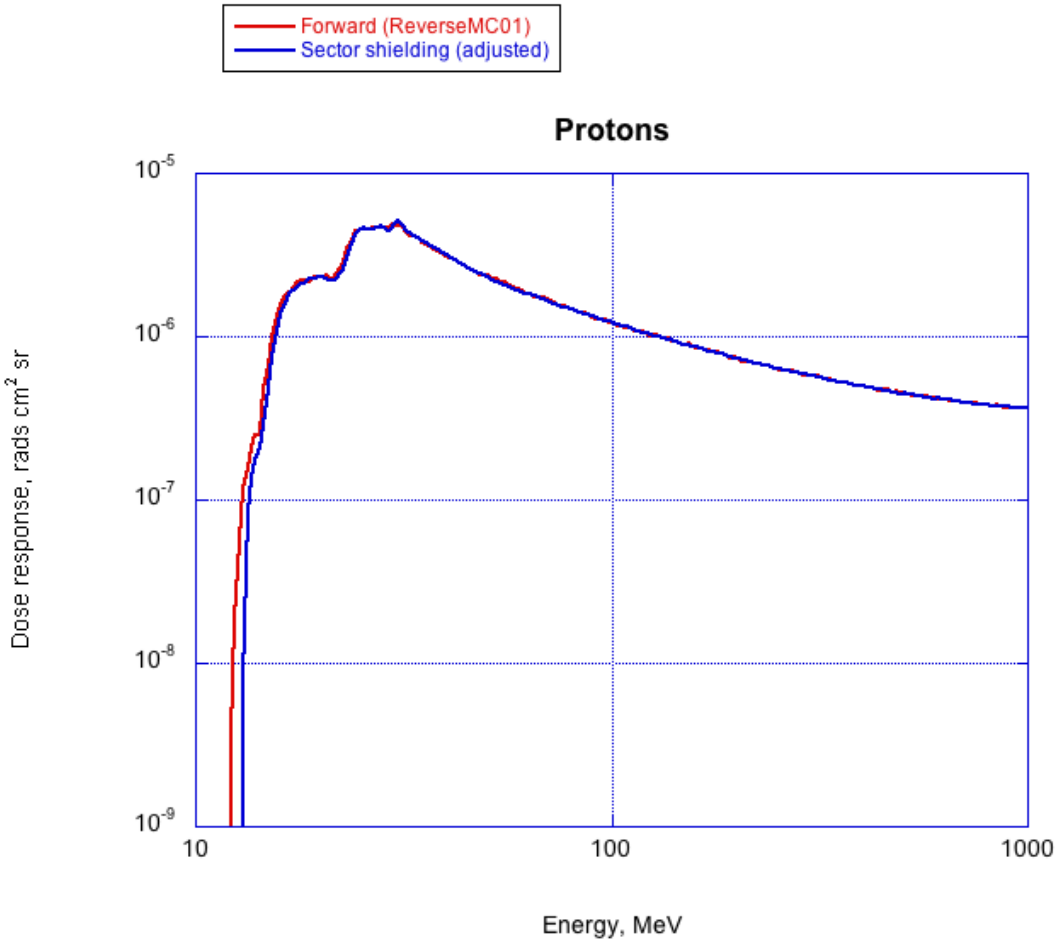

Thus we made the further modification of adjusting the contribution to the column mass density sum of each material, scaling its thickness by an appropriate ratio to match the range in aluminum around 100 MeV proton energy (typical of penetration energies for this structure). Agreement with forward calculation is not perfect, but it is much improved; this will give more accurate dose rate calculations where the proton spectrum falls steeply, so that the different thresholds in the curve (penetrating different structures) take effect at the right energies.

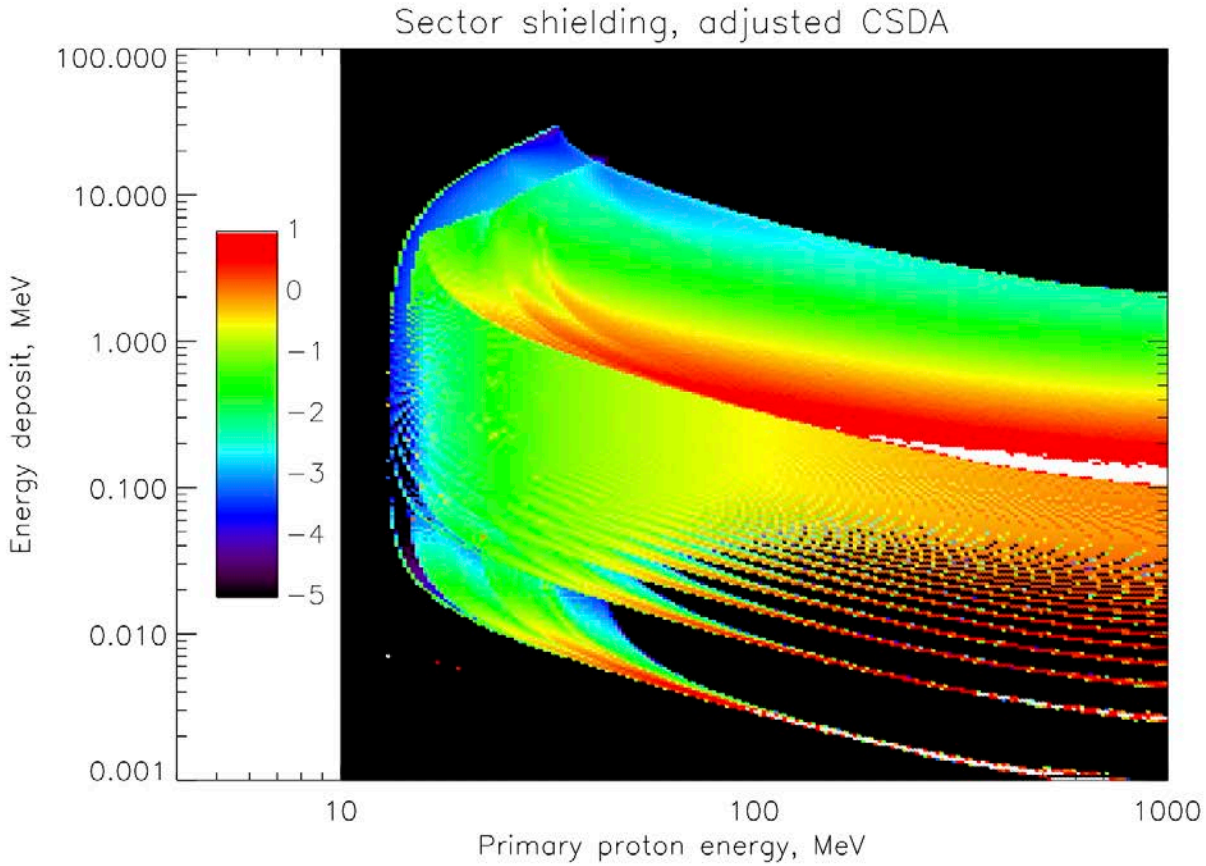

Finally, we show the energy deposit response using the modified sector-shielding calculation. Round-off (digitization) errors cause the stripes at lower energy deposits, though this can be smoothed out, and of course the secondary-electron patch at lower left is missing, but the main features are all present at the right locations and magnitudes.

Please ask me for a copy of the Aerospace Technical Reports for more details, if desired.